Lattice Boltzmann simulations on the role of channel structure for reactive capillary infiltration

Danilo Sergi,* Loris Grossi, Tiziano Leidi, and Alberto Ortona
University of Applied Sciences SUPSI, The iCIMSI Research Institute, Galleria 2, CH-6928 Manno, Switzerland
(Dated: May 22, 2015)

It is widely recognized that the structure of porous media is of relevance for a variety of mechanical and physical phenomena. The focus of the present work is on capillarity, a pore-scale process occurring at the micron scale. We attempt to characterize the influence of pore shape for capillary infiltration by means of Lattice Boltzmann simulations in 2D with reactive boundaries leading to surface growth and ultimately to pore closure. The systems under investigation consist of single channels with different simplified morphologies: namely, periodic profiles with sinusoidal, step-shaped and zig-zag walls, as well as constrictions and expansions with rectangular, convex and concave steps. This is a useful way to decompose the complexity of typical porous media into basic structures. The simulations show that the minimum radius alone fails to characterize properly the infiltration dynamics. The structure of the channels emerge as the dominant property controlling the process. A factor responsible for this behavior is identified as being the occurrence of pinning of the contact line. It turns out that the optimal configuration for the pore structure arises from the packing of large particles with round shapes. In this case, the probability to have flow paths wide and straight is higher. Faceted surfaces presenting sharp edges should be avoided because of the phenomenon of pinning near narrow-to-wide parts. This study is motivated by the infiltration of molten metals into carbon preforms. This is a manufacturing technique for ceramic components devised to advanced applications. Guidelines for experimental work are discussed.

Keywords: Porosity, Microstructure, Capillary infiltration, Lattice Boltzmann simulations, Liquid silicon infiltration

arXiv:1409.0954v2 [cond-mat.soft] 21 May 2015

1. INTRODUCTION

A porous medium is a material presenting some void content in the solid matrix (Dullien, 1992). The fraction of void space defines the porosity ε. Common examples of porous materials include wood (Jeje and Zimmermann, 1979; Ota et al., 1995; Studart et al., 2006) and building materials (Martys and Hagedorn, 2002). For the latters the porosity is exploited in order to trap air with the purpose to achieve better thermal insulation (Dullien, 1992). Soil science is another fruitful research area in the field (Pan et al., 2004; Schaap et al., 2007; Sukop and Or, 2004). In materials engineering, the porosity can also be a key factor in order to meet the highest demands in a variety of applications (Clyne et al., 2006; Furler et al., 2012a and 2012b; Goodall and Mortensen, 2013; Roberts and Garboczi, 2000; Trimis et al., 2006; Zeschky et al., 2005). In general, the pore structure is recognized to have a prominent role for the operating behavior of the material.

In the present work we are concerned with the capillary properties of porous materials. Capillarity is the phenomenon responsible for the spontaneous infiltration of a liquid into a porous medium. It is a pore-scale process arising from the adhesive forces between the liquid and solid phases. Computational fluid dynamics (CFD) relying on the finite element method (FEM) allows to address such problem (Chibbaro et al., 2009c; Svihla and Xu, 2006; Xu and Guetari, 2004). Our study is based on simulations using the Lattice Boltzmann (LB) method in 2D (Benzi et al., 1992; Chen and Doolen, 1998; Succi, 2009; Sukop and Thorne, 2010; Wolf-Gladrow, 2005). This approach has been gaining consideration for handling hydrodynamic systems out of equilibrium involving complex boundaries and interfacial phenomena. More generally, many applications can be figured out in the incompressible limit, i.e. at low Mach numbers (Ghosh et al., 2012; Guiet et al., 2011; Haghani et al., 2013).

The motivating problem for our investigation is the reactive infiltration of molten silicon (Si) into carbon (C) preforms (Bougiouri et al., 2006; Dezellus and Eustathopoulos, 2010; Dezellus et al., 2003; Einset, 1996 and 1998; Eustathopoulos et al., 1999; Hillig et al., 1975; Israel et al., 2010; Liu et al., 2010; Messner and Chiang, 1990; Mortensen et al., 1997; Voytovych et al., 2008). This process is of special relevance for the industrial practice dependent on the processing of carbon and graphite materials (Gadow, 2000; Gadow and Speicher, 2000; Krenkel, 2005; Paik et al., 2002; Salamone et al., 2008). Specifically, ceramization through liquid Si infiltration, or impregnation, is necessary for high-temperature applications such as tribology (Gadow, 2000). In this process, the reaction between Si and C to form silicon carbide (SiC) has been the subject of intense research activity since it coincides with a wetting transition (Bougiouri et al., 2006; Dezellus and Eustathopoulos, 2010; Dezellus et al., 2003; Einset, 1996 and 1998; Eustathopoulos et al., 1999; Hillig et al., 1975; Israel et al., 2010; Liu et al., 2010; Messner and Chiang, 1990; Mortensen et al., 1997; Voytovych et al., 2008). In other words, without this reaction, infiltration would not occur (Bougiouri et al., 2006). Importantly, the formation of SiC can lead to the thickening of the surface behind the invading front (contact line) (Bougiouri et al., 2006; Einset, 1996 and 1998; Israel et al., 2010). Surface growth can result in retardation effects and ultimately hinder the impregnation because of pore obstruction (Bougiouri et al., 2006; Einset, 1996 and 1998; Israel et al., 2010; Messner and Chiang, 1990). In the LB framework, the surface reaction is treated as a precipitation process (Kang et al., 2007, 2002b, 2003, 2004; Lu et al., 2009; Sergi et al., 2014). In this model, the driving mechanism for surface growth is exhaustively compliant with the requirement of mass conservation (Kang et al., 2007). Among

*Corresponding author. E-mail: danilo.sergi@icimsi.ch

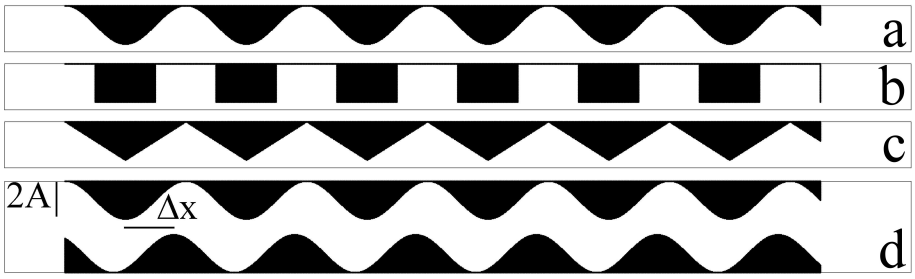

Figure 1: Periodic profiles for the upper wall: that is, sinusoidal profile, rectangular step and zig-zag profile. The last figure shows the case of a sinusoidal capillary with the lower wall misaligned with respect to the upper one. A is the amplitude of the profiles and Δx denotes the displacement inducing misalignment. Similar definitions apply also for the other geometries.

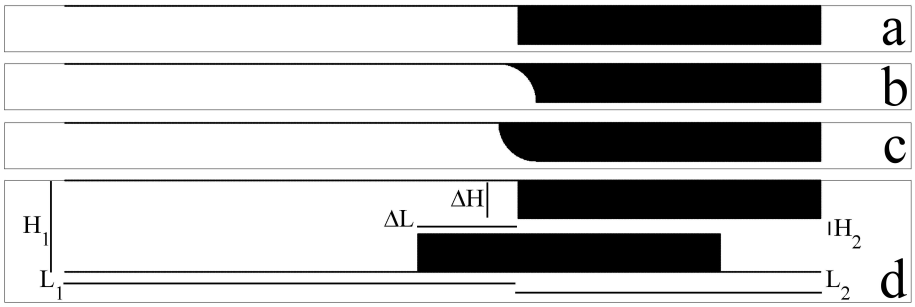

Figure 2: Constricted channel with rectangular, convex and concave junction (upper wall). In the last panel, $L = L_1 + L_2$ is the overall length of the interstice, H_1 is the radius of the first segment, H_2 that of the second one, $\Delta H = (H_1 - H_2)/2$ the width of the solid phase and ΔL the displacement introducing misalingnment between the upper and lower walls. Similar definitions hold also for the capillaries with expansion.

the pioneering works for this subject the article by Miller and Succi (2002) deserves attention.

A porous medium can be regarded as a network of capillary channels. For the sake of clarity, we shall still limit ourselves to single capillaries. In general, the analysis of more complex geometries is based on the theoretical results for this kind of systems. In a previous work (Sergi et al., 2014), we investigated the retardation effects induced by surface growth for the linear Washburn law for interstices of uniform radii. The linear time dependence for the infiltration depth is characteristic of reactive Si infiltration (Israel et al., 2010; Voytovych et al., 2008). It is important to note that the employed LB models (Chibbaro, 2008; Chibbaro et al., 2009b; Diotallevi et al., 2009a and 2009b) only reproduce the macroscopic behavior observed in experiments without providing any explanation for its origin (Israel et al., 2010; Voytovych et al., 2008).

Here, attention is paid to simplified channel structures consisting of single capillaries with different geometric attributes. Namely, we consider periodic profiles (Gern and Kochendörfer, 1997; Patro et al., 2007) with varying degrees of angularity and tortuosity (Duda et al., 2011; Matyka and Koza, 2012). These patterns could arise for example from the juxtaposition of medium-sized C grains. The patterns resulting from the juxtaposition of larger C grains are instead modeled as capillary systems with constrictions or expansions (Einset, 1996). Also in this case, the results for different morphologies and degrees of tortuosity are analyzed.

Our simulations confirm previous results for a uniform channel (Sergi et al., 2014), pointing out that the infiltration velocity affects marginally the process of surface growth and pore closure. The main result of the present study consists in a system of rules for the evaluation of the response of microstructures of different characteristics to capillary infiltration and surface growth. For ceramic products (Gadow, 2000; Gadow and Speicher, 2000; Krenkel, 2005; Paik et al., 2002; Salamone et al., 2008), these are competing phenomena both important in order to obtain complete densification and optimize the final properties. As explained before, the complexity of fully-developed porous systems is decomposed into basic structures. In the following, a comparative analysis is proposed in order to understand the role of the various structural features. Precisely, we shall address questions such as front dynamics, flow retardation, thickening of the surface, pore closure, analysis of characteristic radii and tortuosity. Notably, it arises that the structure of the channels can affect significantly the resulting effective radius. There appears that our findings provide useful inputs for preform preparation. The optimal configuration for the porosity is that containing the larger number of constrictions since the effect of surface growth is weaker. They could realize a percolating network allowing to guide the flow into the porous preforms. Another advantage of this configuration is that it requires coarse particles and so it should be easier to obtain the desired arrangement. Of course, these guidelines need to be verified and improved by more simulation work before to proceed to tests by experiments.

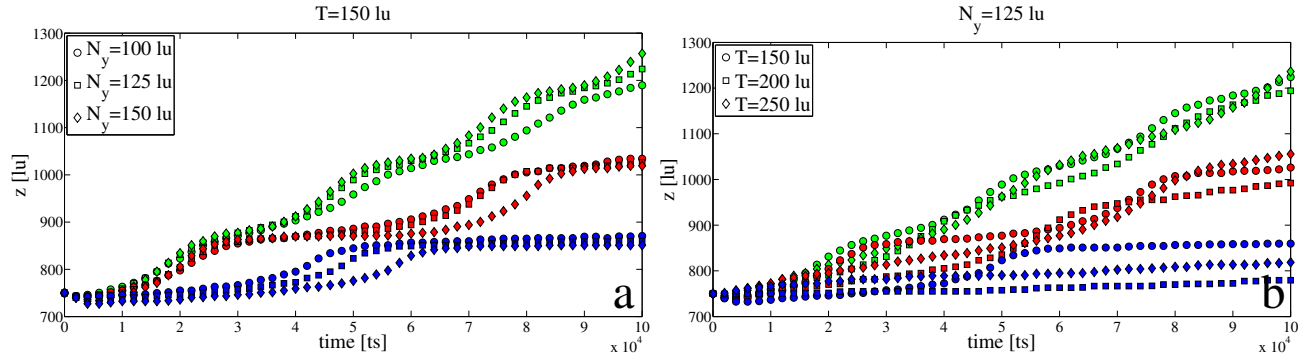

Figure 3: Centerline position z of the advancing front in the course of time for sinusoidal capillaries of length $L = 750$ lu without surface reaction. Color code based on the amplitude A. We use green, red and blue for increasing amplitude $A = i(N_y - 25)/16$, where $i = 2, 3, 4$.

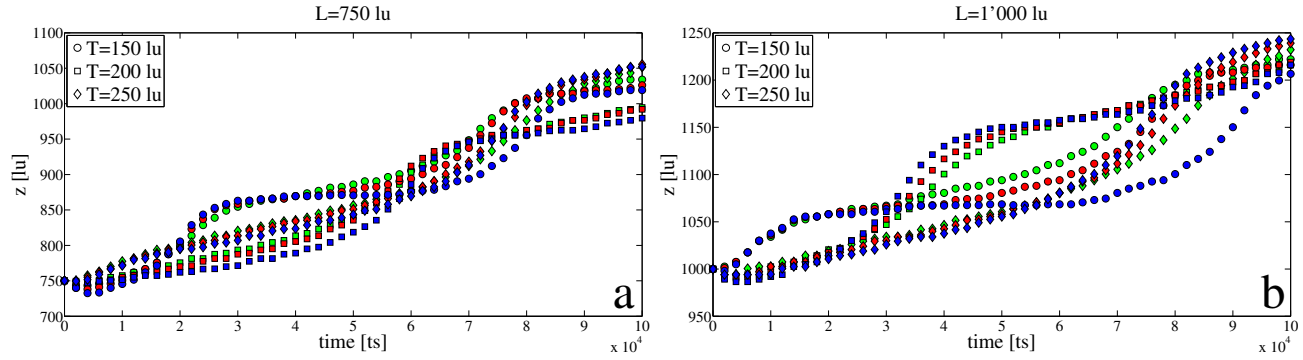

Figure 4: Time dependence of the centerline position z of the invading front in the absence of reaction for sinusoidal profiles. Color code based on the domain width N_y: green, red and blue for increasing values $N_y = 100, 125, 150$ lu. The systems have the average minimum height $< H_{\min} >= 50$ lu, determined using the amplitude $A = 3(N_y - 25)/16$.

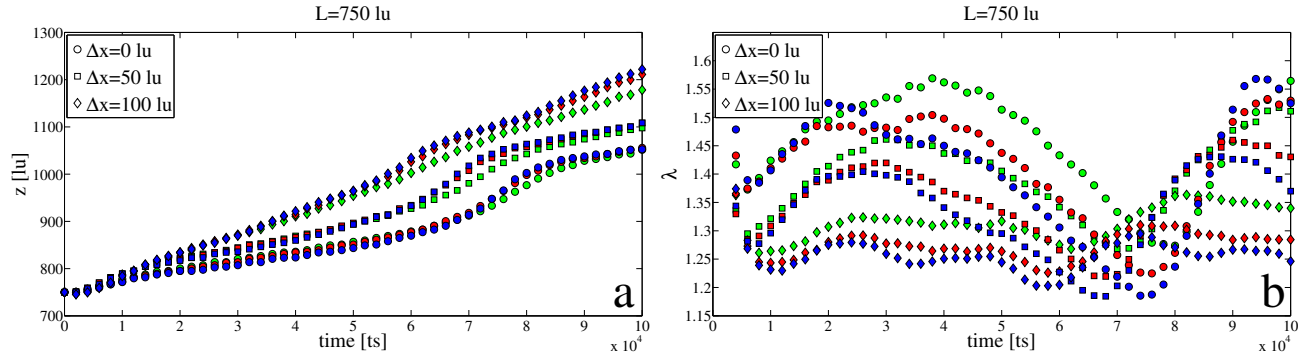

Figure 5: Sinusoidal capillary systems without reaction in the presence of misalignment between the walls (see Fig. 1). Color code based on the domain width N_y: green, red and blue for $N_y = 100, 125, 150$ lu, respectively. The period is set to $T = 250$ lu, while the amplitude is given by $A = 3(N_y - 25)/16$, providing the average minimum height $< H_{\min} >= 50$ lu. (a) Evolution of the centerline position z of the meniscus. (b) Evolution of the tortuosity λ.

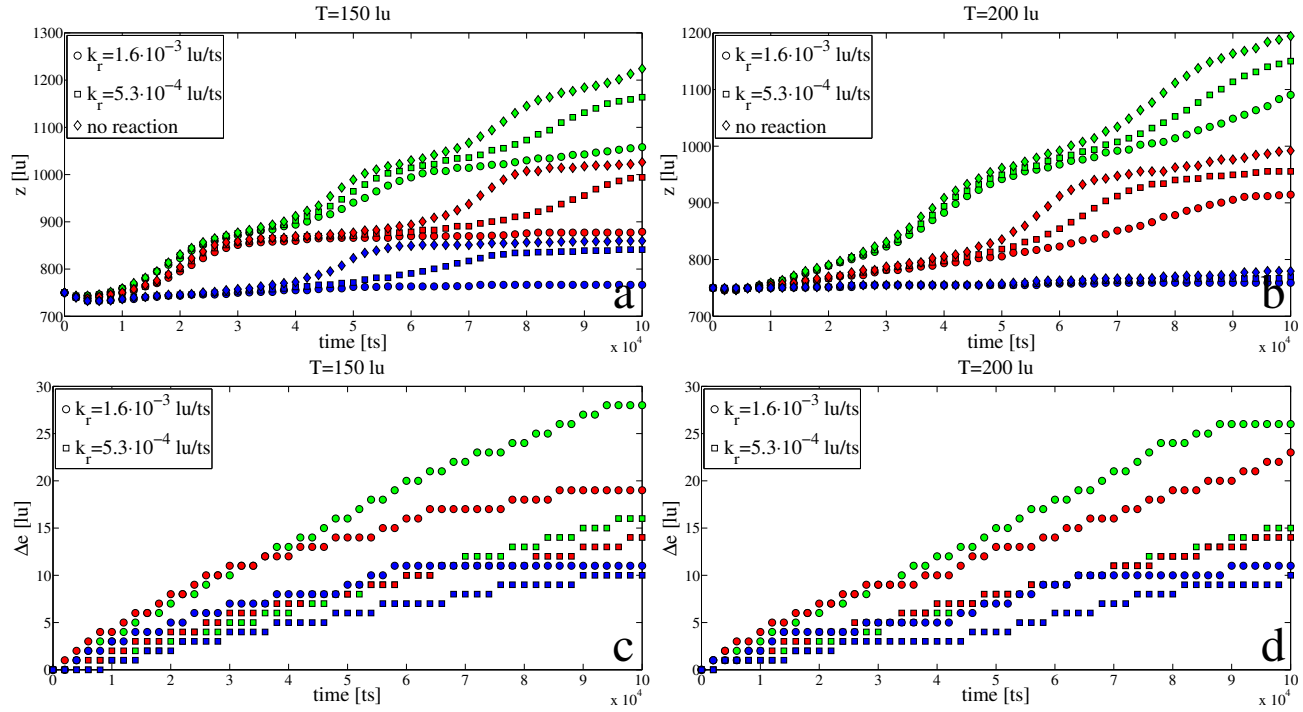

Figure 6: Results for sinusoidal capillary systems of length $L = 750$ lu with $N_y = 125$ lu in the presence of surface reaction, controlled by the reaction-rate constant k_r. Color code based on the amplitude $A = i(N_y - 25)/16$ with $i = 2,3,4$, for green, red and blue, respectively. Top: Time dependence of the invading front. Bottom: Maximal thickening Δe of the solid surface in the course of time.

2. LB MODELS

The LB method can simulate hydrodynamic phenomena at a mesoscopic level: streaming and collision processes are reminiscent of the particulate nature of liquids, demanding nevertheless for a statistical treatment. More precisely, the velocity space is discretized and distribution functions account for the particles moving along a given direction (Benzi et al., 1992; Chen and Doolen, 1998; Succi, 2009; Sukop and Thorne, 2010; Wolf-Gladrow; 2005). In the present work we employ the same models as in Sergi et al. (2014) with the same notation and terminology. More details can be found in the related literature. Namely, fluid flow is treated by means of multicomponent models (Chibbaro, 2008; Chibbaro et al., 2009b; Diotallevi et al., 2009a and 2009b). For solute transport and reactive boundaries we follow closely Kang et al. (2007). For similar works the interested reader is addressed to the articles by Kang et al. (2002b, 2003, 2004) and Lu et al. (2009).

In the sequel, we shall express the simulation results in model units. The basic units are those of mass, length and time; in symbols, mu, lu and ts, respectively (Sukop and Thorne, 2010). Ordinary units are obtained after suitable transformations (Gross et al., 2010; Lu et al., 2009). Of course, comparative analyses with experiments based on dimensionless parameters (Reynolds, Damkohler, Peclet, capillary, Bond, Weber numbers, etc.) are preferable. These numbers allow to establish equivalences between systems (Landau and Lifshitz, 2008) and have the same value in the common systems for units like the SI.

3. CAPILLARY SYSTEMS AND SIMULATION SETTINGS

Wetting and infiltration studies have highlighted the relevance of surface and pore microstructure (Alava et al., 2004; Grzelakowski et al., 2009; Quéré, 2008). The importance of pore characteristics has gained general acceptance also for the processing route of C/SiC composites (Gadow and Speicher, 2000; Israel et al., 2010; Paik et al., 2002; Salamone et al., 2008). One way to control the pore properties of the matrix is via the enrichment by ceramic powders. Our interest resides in the optimization of the infiltration process taking into account surface reactivity and subsequent thickening. We investigate basic, simplified capillary geometries that could arise from intra-particle porosity. In a general porous medium, the pores do not have a constant cross-section. Furthermore, it is possible to identify larger void spaces. To start with, we thus consider capillaries presenting the alternation between wide and narrow portions. Aligned periodic walls reproduce structures with such properties (Gern and Kochendörfer, 1997; Patro et al., 2007). Our focus is on the sinusoidal profile. Other geometries are also considered, that is, rectangular steps and zigzag walls. The degree of tortuosity is modified by introducing a misalignment between the upper and lower walls. Figure 1 illustrates some representative geometries for this type of systems. Another complication arises from the fact that the pore size distribution is generally to some extent broad. In order to undestand how this aspect can affect capillary impregnation, simulations are performed also for capillaries with constrictions or expansions. The step at the junction can be rectan-

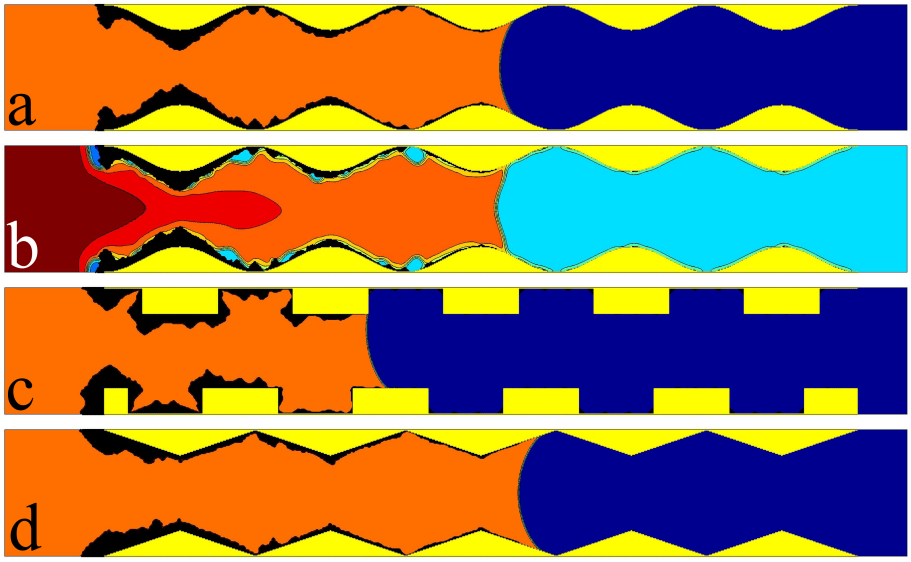

Figure 7: Periodic systems after 60′000 timesteps with channel width $N_y = 125$ lu, capillary length $L = 750$ lu, period $T = 150$ lu, amplitude $A = (N_y - 25)/8$, corresponding to $H_{\min} = 75$ lu, and reaction-rate constant $k_r = 1.6 \cdot 10^{-3}$ lu/ts. Unless stated otherwise, the figures represent fluid flow with color code based on the density of the wetting component. Dark points for the phase resulting from surface growth and yellow points for the initial solid phase. (a) Sinusoidal profile. (b) Sinusoidal profile. Representation of solute transport with color code based on the solute concentration. (c) Step-shaped profile with misalignment given by $\Delta x = 100$ lu. (d) Zig-zag profile.

gular, convex or concave. Also in this case, the tortuosity of the systems is varied. Examples for this type of systems are shown in Fig. 2. Loosely speaking, a low degree of angularity is for example representative of directly synthesized powders, while a higher degree of angularity can be observed for milled powders.

For the implementation of the various capillary systems we proceed as follows. The simulation domains are N_x long and N_y wide. The length of the capillaries is indicated by L and their height by H. For all systems we have $L = N_x/2$. The left extremity of the capillary coincides always with the point $x_s = 2N_x/5$. The periodic profiles are defined by the period T, the amplitude A and the displacement Δx controlling the misalignment between the walls. Since the minimum of the profiles corresponds to the starting point of the solid phase, the amplitude A is equal to half the maximal initial width of the solid phase (see Fig. 1). As an example, the lower wall of the sinusoidal capillary is described by the function $f(x) = A\sin(\omega\tilde{x} + 3\pi/2) + A$ with $\omega = 2\pi/T$ and $\tilde{x} = x - x_s - \Delta x$. These parameters can take on the following values: $L = 750, 1'000, 1'250$ lu, $N_y = 100, 125, 150$ lu, $T = 150, 200, 250$ lu, $A = (N_y - 25)/8, 3(N_y - 25)/16, (N_y - 25)/4$, $\Delta x = 0, T/5, 2T/5$. The choice for the amplitude A guarantees that the width of the necks is at least of 25 lu.

For constricted channels and expansions, the overall length of the capillary is still denoted by L. The length of the first segment, wider or narrower, is indicated by L_1 and that of the second one by L_2; of course, $L = L_1 + L_2$. The other parameters characterizing these systems are the width of the first segment H_1, that of the second part H_2, the width of the step $\Delta H = (H_1 - H_2)/2$ (for constrictions) and the displacement ΔL introducing a misalignment between the two walls (see Fig. 2). The convex and concave shapes for the step are defined using circles of center (x_c, y_c) and radius $r = \Delta H$. For the lower wall, the coordinates of the center are given by $x_c = 2N_x/5 + L_1 \mp \Delta H/2 - 1$ and $y_c = \Delta H$ (the signs refer to the convex and concave shapes respectively). The various parameters can vary as follows: $L = 750, 1'000, 1'250$ lu, $H_1 = 100, 125, 150$ lu, $L_1 = 2L/5, 3L/5, 4L/5$, $\Delta H = (N_y - 25)/4, 3(N_y - 25)/8, (N_y - 25)/2$, $\Delta L = 0, L_2/3, 2L_2/3$ with $\Delta L < L_1$ (for constrictions). Furthermore, the step at the junction can have a rectangular, convex or concave shape (see Fig. 2).

Our systems consist of binary mixtures (Chibbaro, 2008; Chibbaro et al., 2009b). In the initial condition, the first component always occupies half of the simulation domain. This means that the first fluid fills the capillary up to one-tenth of its length. The density values are chosen so that $\rho_0 = \rho_1 + \rho_2 = 2$ mu/lu^2 and $\rho_1/\rho_2 = 2.5\%$, where the first fluid is the main component; elsewhere the ratio between the densities of the two components is inversed. Unless stated otherwise, the parameter for fluid-fluid interactions (cohesive forces) is $G_c = 0.9$ lu/mu/ts^2, for which the surface tension turns out to be $\gamma = 0.16403$ lu·mu/ts^2 (Sergi et al., 2014). Solid-fluid interactions are instead determined by the parameters $G_{ads,1} = -G_{ads,2} = -0.35$ lu/ts^2. In so doing, the first component wets the solid phase while the second one is a non-wetting fluid. These settings (Sergi et al., 2014) reproduce an equilibrium contact angle around 30° typical for droplets of molten Si on SiC substrates (Bougiouri, et al., 2006; Voytovych et al., 2008). Regarding solute transport, we proceed as done by Sergi et al. (2014). In the initial configuration, in the region filled with the first fluid component, the wetting one, the solute concentration is $C_1 = 10^{-2}$ mu/lu^2; elsewhere

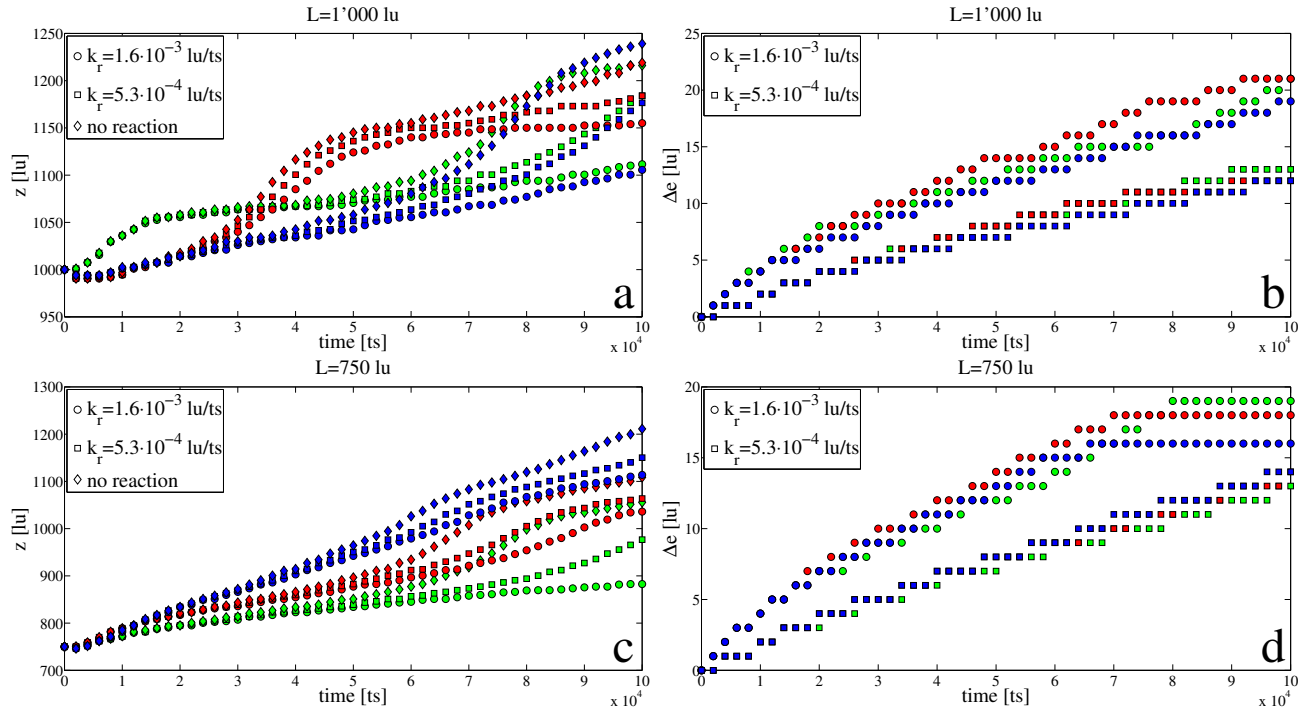

Figure 8: Sinusoidal capillary systems with reactivity enabled, adjusted via the reaction-rate constant k_r. The domain width is set to $N_y = 125$ lu and the amplitude is kept fixed at $A = 3(N_y - 25)/16$, yielding the minimum height $H_{\min} = 50$ lu. Top: Color code based on the period T: green, red and blue for $T = 150, 200, 250$ lu, respectively. Bottom: Color code based on the parameter Δx controlling the misalignment between the walls: green, red and blue for $\Delta x = 0, 50, 100$ lu. The period is $T = 250$ lu.

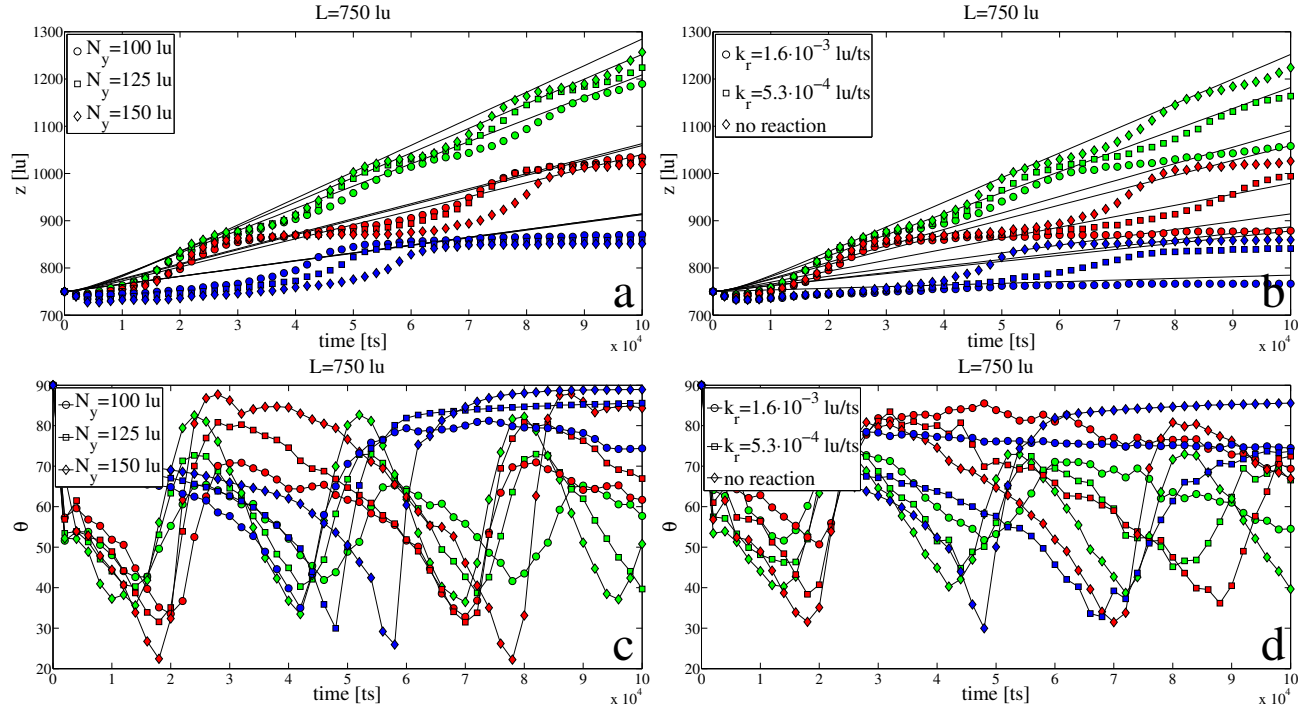

Figure 9: Sinusoidal capillary systems of period $T = 150$ lu. Points for simulation results; the solid lines are determined using Eq. 1. (a) The solid surface is inert. Color code based on the amplitude A: green, red and blue for $A = i(N_y - 25)/16$ with $i = 2, 3, 4$, respectively. (b) The surface reaction is controlled via the reaction-rate constant k_r. The domain width is $N_y = 125$ lu. Color code based on the amplitude $A = i(N_y - 25)/16$, with $i = 2, 3, 4$, corresponding to green, red and blue, respectively. (c) Dynamic contact angle for the conditions of a. (d) Dynamic contact angle for the systems of b.

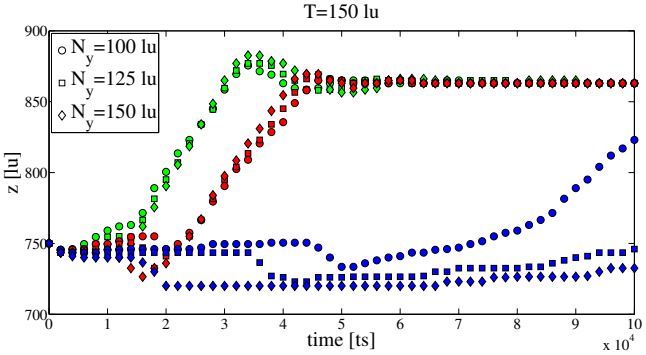

Figure 10: Front displacement in the course of time for step-walled capillaries without reaction. The length of the capillary is $L = 750$ lu. Color code based on the amplitude A. It is given by $A = i(N_y - 25)/16$ with $i = 2,3,4$, corresponding to the colors green, red and blue, respectively.

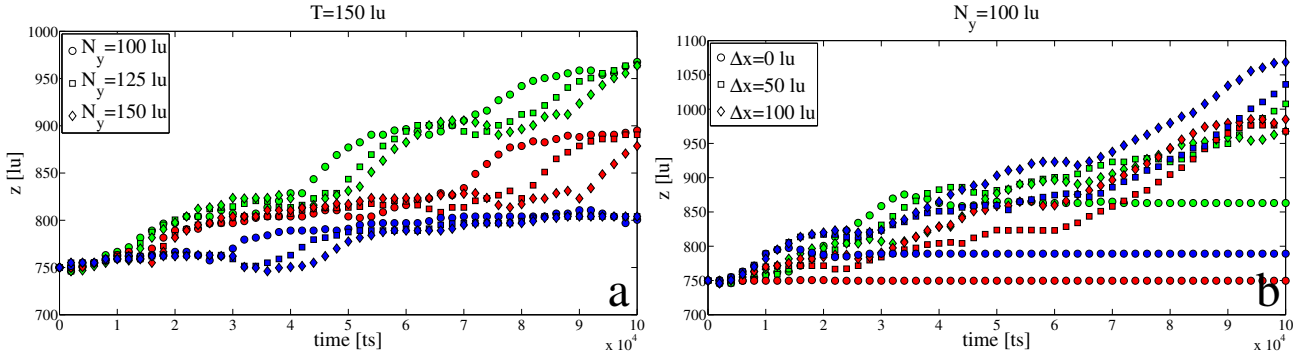

Figure 11: Centerline position of the invading front in the course of time for capillary systems with periodic step-shaped walls in the absence of surface reaction. The capillaries have length $L = 750$ lu. (a) The misalignment between the walls is $\Delta x = 100$ lu. Color code based on the amplitude $A = i(N_y - 25)/16$ with $i = 2,3,4$ for green, red and blue, respectively. (b) The amplitude is fixed to $A = (N_y - 25)/8$, determining the minimum height $H_{\min} = 62$ lu. Color code based on the period: $T = 150, 200, 250$ lu for green, red and blue.

the solute concentration is $C_2 = 2 \cdot 10^{-3}$ mu/lu^2. The parameters for the function introducing an interface for solute are assumed to be $G_s = -4.875 \cdot 10^{-3}$ mu/lu/ts^2, $\varphi_0 = 1$ and $C_0 = 4.9 \cdot 10^{-3}$ mu/lu^2 (Sergi et al., 2014). For the saturated concentration we choose $C_s = 5 \cdot 10^{-3}$ mu/lu^2. At the beginning, the mass deposited on solid boundaries is $b_0 = 2 \cdot 10^{-3}$ mu; the threshold value determining surface growth is $b_{\max} = 10^{-2}$ mu. The relaxation time for solute transport is set to $\tau_s = 1$ ts, so the diffusion coefficient D is kept fixed. The reaction-rate constant is varied according to the rule $k_r = (8/5)/I$ with $I = 1'000, 3'000$ ts. We recall that the Damkohler number is defined as $Da = k_r N/D$ (Kang et al., 2003 and 2004; Lu et al., 2009), where N is a characteristic length for the system. Last, the evolution of every system amounts to $100'000$ ts. For the analysis, 50 evenly-spaced frames are collected. The interfaces are tracked as explained in the article by Sergi et al. (2014). Here the interested reader can also find more details about the motivations for the simulation settings.

4. RESULTS AND DISCUSSION

4.1 Periodic profiles

Periodic profiles give rise to capillaries with a rich variety of morphology characteristics (see Fig. 1). Simply said, with T variations the pore chambers and necks become longer, for increasing values. Increases in the amplitude A lead to deeper pore chambers (wider stomaches) and narrower necks (closer tips). With increasing values of Δx the pore chambers become less wide and the necks are less long. Moreover, the path connecting adjacent maxima and minima is shorter for the zig-zag and sinusoidal profiles while it is longer for the rectangular steps.

4.1.1 Sinusoidal profiles

To start with, let us consider sinusoidal profiles in the absence of surface reaction. Figure 3 shows the behavior of the invading front in the course of time for varying channel width N_y, period T and amplitude A. In general, it is possible to distinguish phases of pronounced acceleration fol-

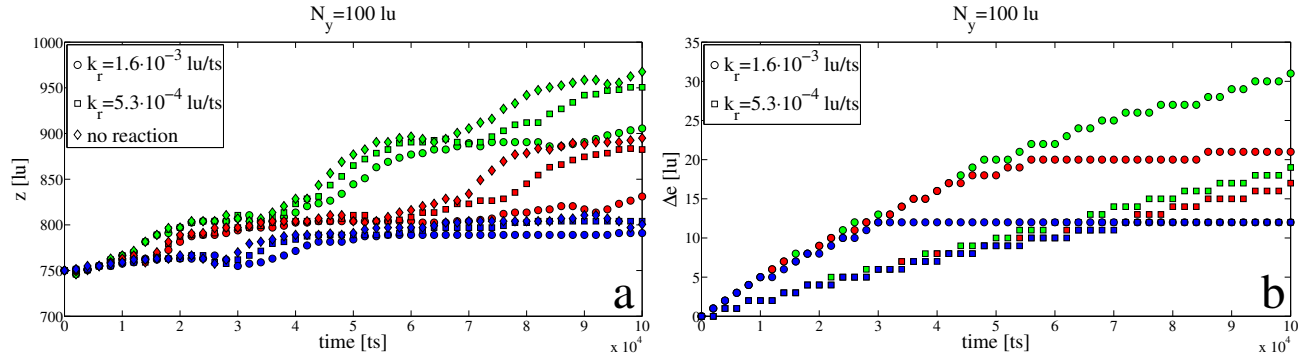

Figure 12: Capillary systems with periodic step-shaped walls in the presence of surface reaction. The period is fixed to $T = 150$ lu and the misalignment is set to $\Delta x = 100$ lu. Color code based on the amplitude: green, red and blue for $A = i(N_y - 25)/16$ when $i = 2,3,4$. (a) Front displacement in the course of time. (b) Evolution of the maximal thickening of the solid surface.

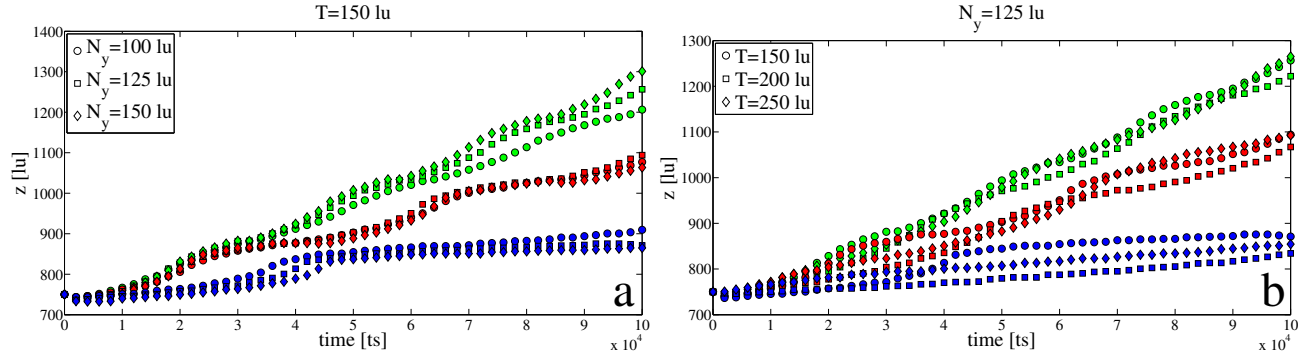

Figure 13: Front dynamics for zig-zag walls in the absence of reactivity. The length of the capillary is $L = 750$ lu. Color code based on the amplitude A: green, red and blue are associated with $A = i(N_y - 25)/16$ where $i = 2,3,4$.

lowed by phases of weaker acceleration leading eventually to plateaus. This phenomenon is usually referred to as pinning of the interface (Blow et al., 2009; Chibbaro et al., 2009a and 2009c; Kusumaatmaja et al., 2008; Mognetti and Yeomans, 2009; Wiklund and Uesaka, 2012 and 2013). Basically, pinning occurs in the proximity of the necks, i.e. close to narrow-to-wide structures. This phenomenon is of course more marked for capillaries having narrower necks. The role of the period is not so clear. It seems that for narrower necks pinning occurs for the smaller period. Increasing periods tend mainly to weaken the capillary forces without enhancing the phenomenon of pinning (results not shown for brevity), as we could verify with longer simulations up to $500'000$ timesteps. It should be noted that for these systems the minimum and maximum radii are the same while the average and hydraulic radii are comparable. The hydraulic radius is defined as $r_h = (1/2)\text{Area}/\text{Perimeter}$ (Dullien, 1992). The plots of Fig. 3 also indicate that the various curves are associated with three distinct infiltration behaviors. It is important to note that the minimum radius is not the same within a group of capillaries. What seems to really matter is rather the ratio of the amplitude to the domain width A/N_y. It follows that to first approximation the infiltration process depends on the structure of the capillary. For the sake of clarity, we consider the quantity $R = < (V - < V >)^2 > / < V >$, where V is a variable and brackets indicate average. Let us consider the data for which N_y varies: if $V = A/N_y$, it is found that R is at least $1'000$ times smaller than for $V = r_{\min}$. Thus, A/N_y characterizes better the infiltration behavior. It really has to be noted that if $T = 150$ lu and $A = (N_y - 25)/8$, the minimum heights are $H_{\min} = 62, 75$ and 87 lu for $N_y = 100, 125$ and 150 lu, respectively. For $N_y = 150$ lu the minimum radius is bigger, but this is not sufficient in order to ease penetration, since the pore chamber becomes deeper (stronger drag force).

Figure 4 refers to capillary systems with varying channel width N_y and period T. It clearly arises that, for a medium value of the average minimum height $< H_{\min} >$, the phenomenon of pinning is accentuated with shorter periods and longer capillary lengths, but this does not result in a strong retardation for capillary infiltration. If we assume that the infiltration velocity is proportional to $1/L$, as for smooth capillaries (Chibbaro et al., 2009b), for the infiltration velocity we can write $v(L+\Delta L)/v(L) \approx (1 - \Delta L/L)$. In passing from $L = 750$ lu to $L = 1'000$ lu, this ratio becomes $v(L+\Delta L)/v(L) = 0.67$. From Fig. 4 there appears that the invading fronts reach almost the same depth. Precisely, on average we find that $v(L+\Delta L)/v(L) = 0.82$; the infiltration velocities are determined by applying the method of least squares. If we restrict our attention to the data for $T = 200$ lu, it even turns out that $v(L+\Delta L)/v(L) = 0.96$. In this case, if we overcome the ob-

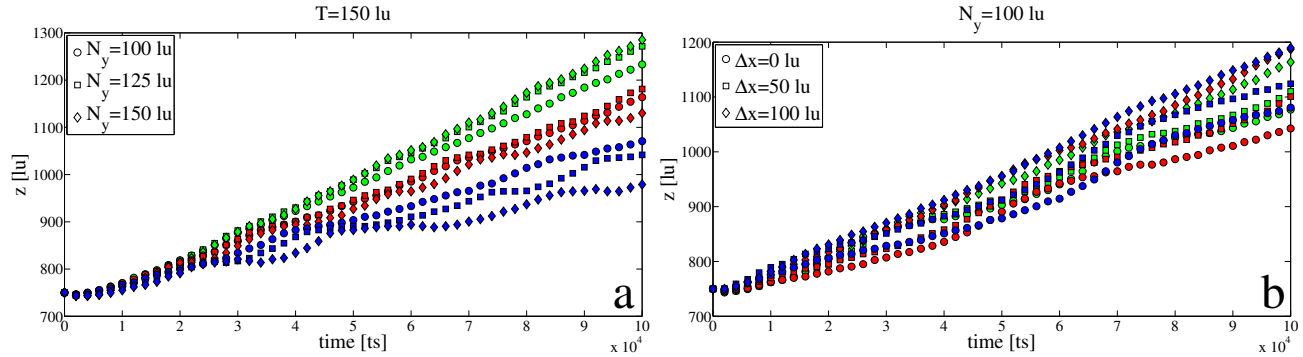

Figure 14: Motion of the invading front for zig-zag walls without reactivity. The capillaries have length $L = 750$ lu. (a) The misalignment between the walls is set to $\Delta x = 100$ lu. Color code based on the amplitude $A = i(N_y - 25)/16$ with $i = 2,3,4$ for green, red and blue. (b) The amplitude is fixed to $A = 3(N_y - 25)/16$. Color code based on the period $T = 150, 200, 250$ lu for green, red and blue.

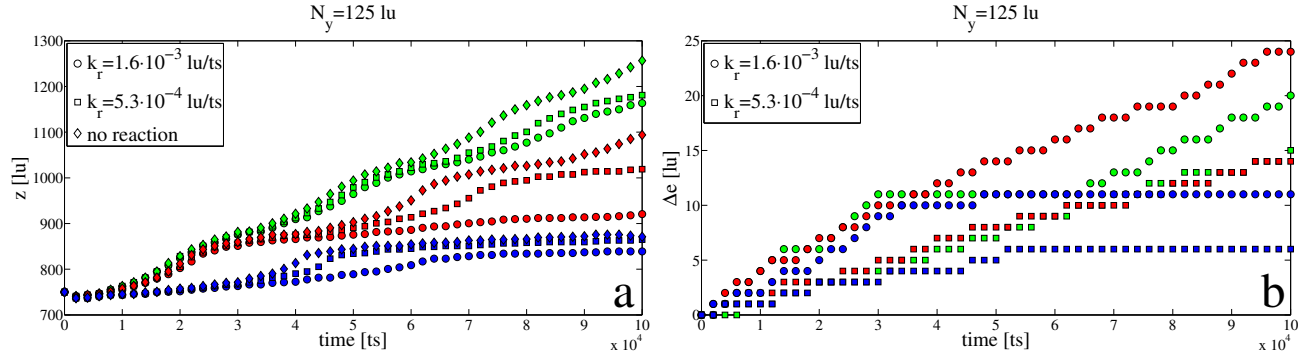

Figure 15: Capillary systems with zig-zag walls in the presence of surface reaction. The length of the capillaries is $L = 750$ lu and the period is set to $T = 150$ lu. Color code based on the amplitude $A = i(N_y - 25)/16$ with $i = 2,3,4$ for green, red and blue. (a) Time dependence of the position of the invading front. (b) Evolution of the maximal thickening of the growing surface.

stacle of estimating the velocity by considering z as a function of L for the time fixed at $t = 100'000$ lu, this phenomenon is clearer. It is found that $z(L+\Delta L)/z(L) = 0.91$ for $L = 750$ lu and $z(L+\Delta L)/z(L) = 0.88$ for $L = 1'000$ lu. As a result, in the case of sinusoidal profiles, the length of the capillaries affects the infiltration process to a weaker extent. The discussion on the results of Fig. 3 is valid also for longer capillaries. Unless stated otherwise, in the sequel the conclusions can be assumed to hold for all capillary lengths.

Shown in Fig. 5 are the results for capillary systems with misalignment between the upper and lower walls (see Fig. 1). The infiltration process is faster for increasing misalignment of the walls. In that respect, it is important to note that for a given value of Δx the minimum and maximum radii vary with N_y within a group of systems displaying similar behavior. In general, there appears that the effect of pinning is weaker for increasing misalignment of the walls. Furthermore, for higher misalignment, it is found that pinning is clearly stronger in the case of narrower necks and small periods (results not shown for brevity). We also consider the tortuosity (Duda et al., 2011; Matyka and Koza, 2012). The tortuosity is a measure of the departure of fluid flow from straight pathways. The calculations are made by means of the formula $\lambda = < u > / < u_x >$ (Duda et al., 2011; Matyka and Koza, 2012), $\boldsymbol{u}$ being the overall fluid velocity (Kang et al., 2002a; Shan and Chen, 1993; Shan and Doolen, 1995). It should be kept in mind that at the interface there are spurious currents (Wagner, 2003). The results shown in Fig. 5 indicate that the tortuosity is smaller for higher misalignment of the walls. This means that it is more important to have wider pathways rather than only narrow, straight ones. The curves are grouped approximately according to the misalignment of the walls.

Figure 6 has to do with sinusoidal capillaries in the presence of reaction. Without reaction, the increase in period T results in a slightly lower penetration depth for $H_{\min} = 75$ and 50 lu. When the reactivity is enabled, no drastic difference for the penetration depth can be observed. In the absence of reaction, in passing from $T = 150$ lu to $T = 200$ lu, flow slows down significantly for $H_{\min} = 25$ lu (cf. discussion on Fig. 3). Again, this points out that the structure of the capillary is more important than the minimum radius (cf. comments on Fig. 3). With surface reaction, the results for the maximal thickening Δe of the solid surface (Sergi et al., 2014) indicates that the process of surface growth is not strongly affected by fluid behavior. The morphology presented in Fig. 7 supports this thesis. This consequence is quite expected since we know that the infiltration velocity was proven to have a marginal role on the kinetics of pore closure (Sergi et al., 2014). There appears an

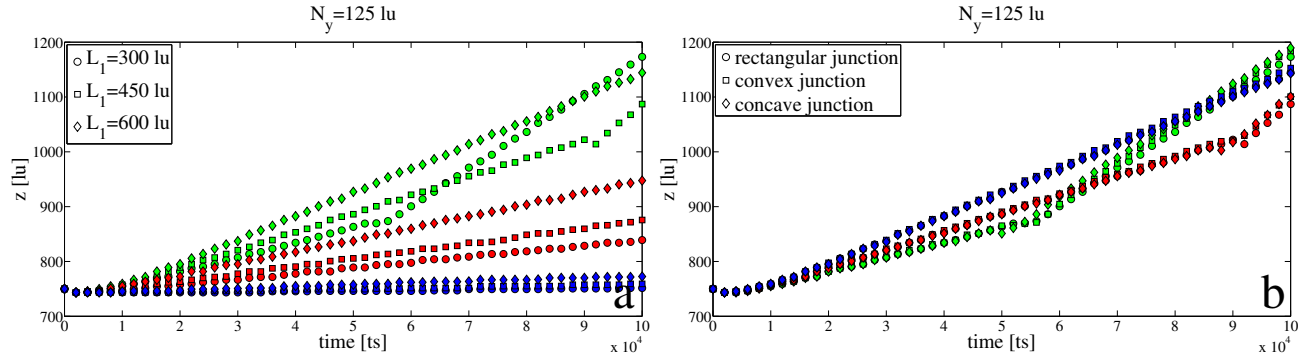

Figure 16: Time dependence of the front position for constrictions without reactivity. The length of the capillary is $L = 750$ lu. (a) The junction has a rectangular shape. Color code based on the width $\Delta H = 25, 38, 50$ lu associated with green, red and blue, respectively. The corresponding minimum heights are $H_{\min} = 75, 50, 25$ lu. (b) The width of the step is set to $\Delta H = 25$ lu. Green, red and blue for the length of the wider segment given by $L_1 = 300, 450, 600$ lu.

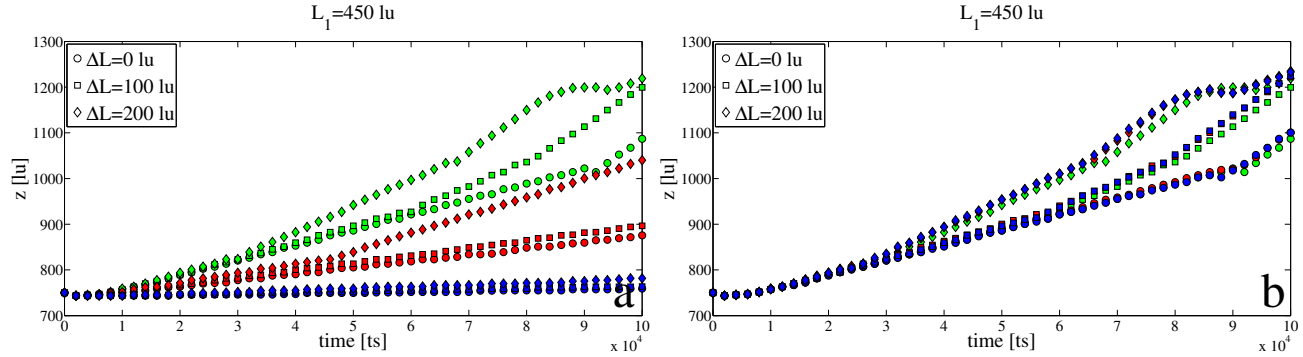

Figure 17: Front dynamics for constrictions with inert solid surface. The length of the capillary is $L = 750$ lu; the width of the simulation domain is $N_y = 125$ lu. (a) Color code based on the width of the solid phase ΔH: green, red and blue for $\Delta H = 25, 38, 50$ lu, leading to the minimum heights $H_{\min} = 75, 50, 25$ lu. (b) The width of the solid phase is $\Delta H = 25$ lu (i.e., $H_{\min} = 75$ lu). Color code based on the shape of the junction: green, red and blue for rectangular, convex and concave.

exception for the system with $H_{\min} = 50$ lu and $k_r = 1.6 \cdot 10^{-3}$ lu/ts. Visual inspection of the dynamics reveals that this difference is chiefly due to an asymmetry in the thickening of the surface near the neck. For other N_y values the curves for Δe have a similar behavior.

In Fig. 8 we analyze the effects of pinning for surface growth. When the period T varies, it is possible to distinguish different infiltration behaviors due to pinning. What is important to remark is that the maximal width of the growing surface Δe is not affected by the hydrodynamic behavior. The evolution of Δe depends essentially on the reaction-rate constant k_r. It is observed that the infiltration process tends to be retarded to a larger extent by surface growth with smaller periods as the plateaus become longer (i.e., pinning more marked). Concerning the results for different tortuosities, from Fig. 8 it can be seen that the various curves can be considered as grouped according to the degree of misalignment. On the other hand, the quantity Δe depends mainly on the reaction-rate constant k_r. These findings give further evidence for the prominence of the capillary structure, while the hydrodynamic behavior is of secondary importance for the occurrence of pore closure. The infiltration process is slowed down by surface growth more significantly for aligned walls.

We recall that for a uniform capillary, in the absence of surface reaction, the process of capillary infiltration is described by the following equation (Chibbaro et al., 2009b):

$$z(t) = \frac{V_{\text{cap}} H \cos\theta}{6L} t_d [\exp(-t/t_d) + t/t_d - 1] + z_0 \ , \quad (1)$$

where $V_{\text{cap}} = \gamma/\mu$ and $t_d = H^2/12\mu$. By z we designate the centerline position of the invading front, γ is the surface tension, μ the dynamic viscosity, ρ the density, H the capillary height, L the length, θ the contact angle. The quantity z has a linear dependence with time. We want to use this formula in order to extract approximations for the effective radius r_{eff}. The well-known result for the capillary pressure $\Delta P = 2\gamma\cos\theta/H$ allows to fit the simulation data to a straight line with a slope given by $H^2\Delta P/12\mu L$. By using for ΔP a suitable average, an estimate for the effective radius can be obtained. From this result, we then calculate the dynamic contact angle using the capillary pressure (Joos et al., 1990; Van Remoortere and Joos, 1993). Finally, by taking an average for the contact angle it is possible to employ Eq. 1, as shown in Fig. 9. Deviations from the behavior predicted by Eq. 1 are more marked when the phenomenon of pinning occurs. The reactivity turns out to enhance the effect of pinning. At the be-

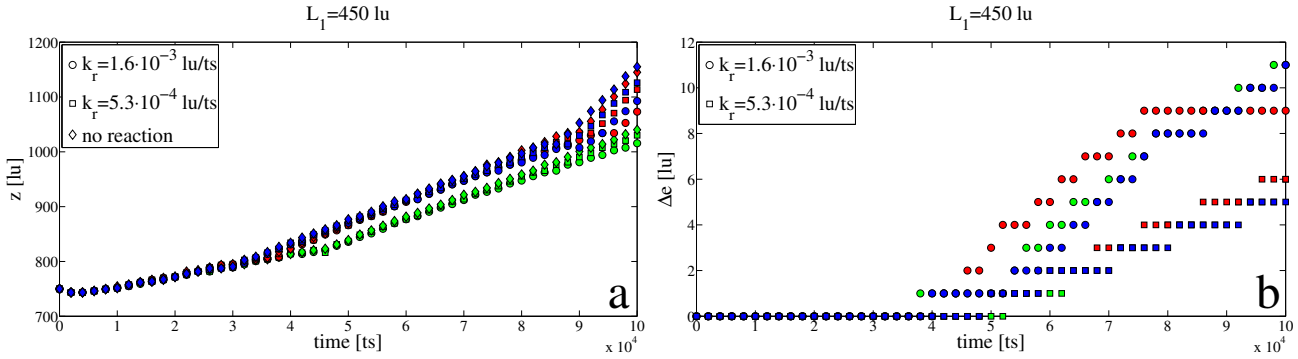

Figure 18: Results for constrictions in the presence of surface reaction. The length of the capillaries is set to $L = 750$ lu, the width of the simulation domain is $N_y = 125$ lu and the misalignment is given by $\Delta L = 200$ lu. The initial width of the solid surface is given by $\Delta H = 38$ lu, corresponding to a minimum height of $H_{\min} = 50$ lu. Color code based on the morphology of the junction: green, red and blue for rectangular, convex and concave. (a) Front position in the course of time. (b) Time dependence of the maximal thickening of the growing surface in the neighborhood of the junction.

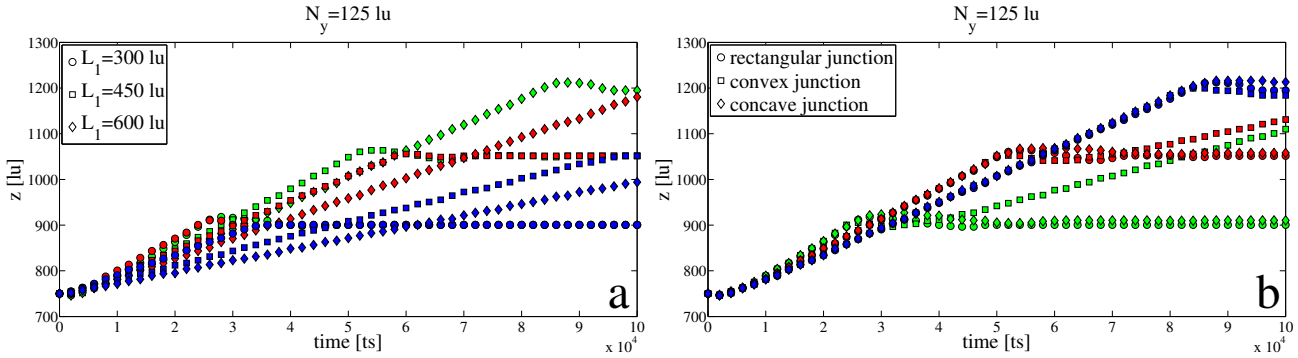

Figure 19: Front position in the course of time for capillary systems with expansions. The surface reaction is disregarded. The length of the capillaries is $L = 750$ lu. (a) The shape of the junction is rectangular. Color code based on the width of the solid phase $\Delta H = 25, 38, 50$ lu for green, red and blue, respectively. These values determine the minimum heights $H_{\min} = 75, 50, 25$ lu. (b) The width of the step is set to $\Delta H = 25$ lu, i.e. $H_{\min} = 75$ lu. Color code based on the length of the narrower segment $L_1 = 300, 450, 600$ lu, corresponding to green, red and blue.

ginning of every plateau the dynamic contact angle θ reaches the local minimum value. When the infiltration accelerates, θ increases sharply. When pinning is more significant, θ remains quite large and then decreases more slowly. This phenomenon is clearer from the results with reaction, for which pinning is stronger. It is found that the effective radius is better approximated by the average radius, with the exception when pinning becomes more significant. In this case $r_{\min}$ is closer to r_{eff}. It is important to recall that pinning depends mainly on the structure: $r_{\min}$ is a parameter among others defining it, as seen before for the discussion related to Fig. 3.

4.1.2 Step-shaped profiles

For periodic step-shaped walls, we limit ourselves to capillaries of length $L = 750$ lu. From Fig. 10 it emerges that the fluid advances no more when the meniscus reaches the zones of enlargement at $x = 865$ lu. This occurs because at the corners the contact line remains pinned. This behavior was ascertained by repeating the simulations for $N_y = 100, 125$ lu with 500′000 timesteps. The same conclusions hold also for longer periods. As seen before, an increase in capillary forces could be obtained by considering smaller ratios A/N_y (Mognetti and Yeomans, 2009). A detailed analysis of the conditions for depinning is outside the scope of the present study: the interested reader is addressed to the existing literature (Blow et al., 2009; Chibbaro et al., 2009a and 2009c; Kusumaatmaja et al., 2008; Mognetti and Yeomans, 2009).

Figure 11 presents the results in the case of misalignment between the upper and lower walls. The effect of misalignment is that the pinning barrier can be overcome and the meniscus does not remain stuck. The curves are grouped as for sinusoidal profiles (see Fig. 3). Different degrees of misalignment do not separate the infiltration behaviors neatly. Moreover, the dependence on the period is not so marked. The infiltration is slightly faster for $T = 250$ lu, the largest period. The results for the other capillary systems lead to the same conclusions. Of course, the infiltration process is slower for step-shaped walls than for sinusoidal profiles. For the considered number of timesteps, the difference amounts to about 100 lu. Furthermore, the systems with period $T = 150$ lu have the

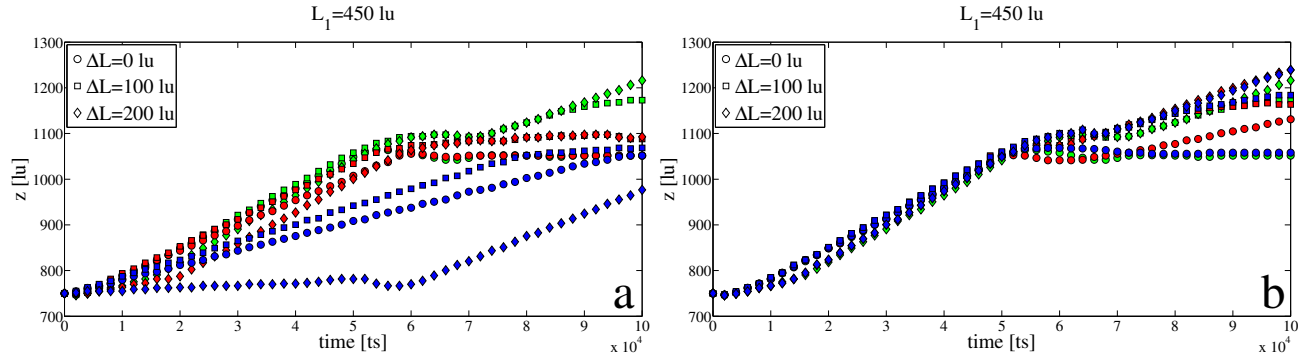

Figure 20: Infiltration dynamics for capillary systems with expansions in the presence of misalignment between the walls. The surface reaction is not taken into account. The length of the capillaries is fixed to $L = 750$ lu and the width of the simulation domain is $N_y = 125$ lu. (a) The shape of the junction is rectangular. Color code based on the width of the solid phase $\Delta H = 25, 38, 50$ lu corresponding to green, red and blue. The minimum heights are thus $H_{\min} = 75, 50, 25$ lu. (b) The width of the step is set to $\Delta H = 25$, leading to $H_{\min} = 75$ lu. Color code based on the shape of the junction: green, red and blue for rectangular, convex and concave, respectively.

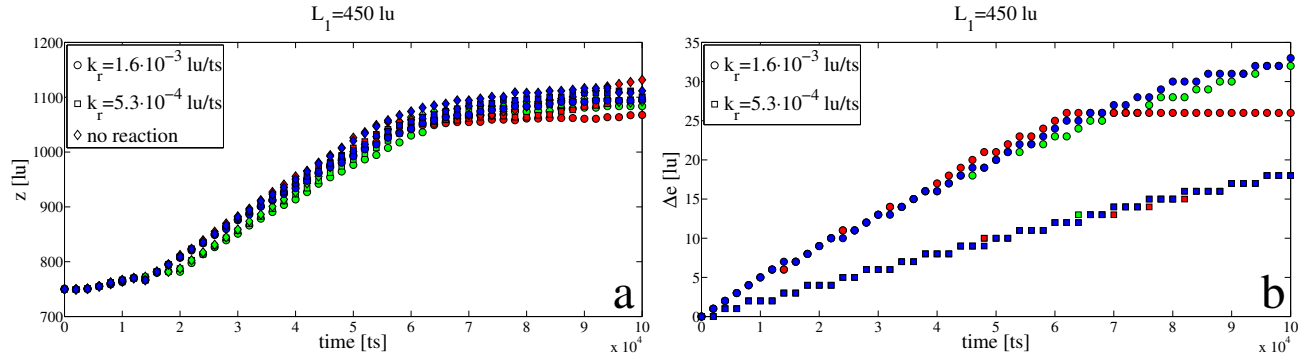

Figure 21: Results for capillary systems with expansions in the presence of surface reaction. The length of the capillaries is $L = 750$ lu, the width of the simulation domain is $N_y = 125$ lu and the misalignment between the walls is set to $\Delta L = 200$ lu. The initial width of the solid step is given by $\Delta H = 38$ lu, determining the minimum height $H_{\min} = 50$ lu. Color code based on the shape of the junction: green, red and blue for a rectangular, convex and concave morphology, respectively. (a) Front position in the course of time. (b) Time dependence of the maximal thickening of the growing surface.

same minimum radius of the sinusoidal capillaries of Fig. 9. It thus follows that the presence of corners quite significantly lowers the effective radius.

The results with reactivity are also in line with previous findings. A typical morphology is shown in Fig. 7. Again, there appears clearly that the quantity Δe, controlling pore closure, does not depend on the flow velocity, as it comes out from Fig. 12. The surface growth opposite to fluid flow seems to have a marginal influence on the infiltration process. The remarks presented in the previous paragraph are material to this statement. The curves of Fig. 12 give further support to this thesis since their behavior is related. Similar results are obtained for the other capillary systems. From a comparison with the equivalent sinusoidal capillary systems it turns out that the process of pore closure occurs sooner with step-shaped walls. Corners are thus more detrimental. Interestingly, it follows that the phenomenon of pore closure is actually sensitive to the wall structure.

4.1.3 Zig-zag profiles

Also for zig-zag profiles we restrict the simulations to the case of capillaries of length 750 lu. In general, the effect of pinning appears to be weaker for this geometry. As it can be seen in Fig. 13, the dependence of z on time is almost linear, with the exception for narrower necks. The curves are grouped as for sinusoidal profiles. But the infiltration process turns out to be faster for zig-zag profiles. The period T does not seem to have a prominent role. For narrower necks, the same conclusions reached for sinusoidal profiles hold (see Fig. 3), as it was verified up to 500′000 timesteps also in this case. Namely, the infiltration depth is almost the same but for larger periods there are less evident plateaus.

The misalignment between the walls has the effect to speed up capillary infiltration especially for narrower necks, as shown in Fig. 14. For wider necks, the advantage of misalignment is comparable to that for the other geometries, that is within 150 lu (see Fig. 5). It is found that the dynamics is slightly faster for larger periods (not shown for brevity); the corresponding characteristic radii (e.g., minimum and hy-

draulic) are almost the same. The other capillary systems lead to the same conclusions.

From Fig. 15 it can be seen that, for the same reaction conditions, Δe does not display approximately the same behavior until pore closure occurs, as for the other profiles (see Figs. 6, 8 and 12). The difference can be ascribed to the fact that the surface does not grow principally near the maximum, i.e. the peak (see Fig. 7). By varying the width of the channels, this phenomenon takes place for other combinations of the other parameters. It is thus difficult to identify the causes with precision. In any case, we can conclude that the process of pore closure results to be slower for zig-zag profiles and this is due to their structural properties (sharp peaks).

Since the infiltration process appears to be slightly faster for zig-zag profiles than for sinusoidal ones, it turns out that the effective radius for this geometry is higher (see Fig. 9), as we could verify. Presumably, the reason resides in the fact that the role of pinning is less significant. However, in general this phenomenon is not captured exhaustively by characteristic radii. Although all periodic profiles have the same minimum radius, in the absence of misalignment, for the step-shaped structure the flow can not proceed. Of course, the tortuosity is expected to be smaller for zig-zag profiles. As an example, for the equivalent systems of Fig. 5, it is found that the first maxima are slightly lower. For completeness, for the equivalent systems with step-shaped structures, the first maxima are around 3 for the highest misalignment of the walls.

4.2 Two-pore systems

Constrictions and expansions are characterized by constant radii (see Fig. 2). In our systems, L_1 determines the relative length of the two segments. ΔH controls the width of the narrower segment. As ΔL increases, the necks become shorter while the main cavity becomes less large. For the rectangular step, at the junction there are two corners. For the convex and concave shapes, there is only one corner, but the profile of the junction is longer.

4.2.1 Constrictions

Also for constrictions the length of the capillary is fixed to $L = 750$ lu. Furthermore, we consider for the width of the simulation domain only the case $N_y = 125$ lu. From Fig. 16 it is interesting to see that for the channels with higher minimum radius, when the capillary shrinks, the flow accelerates. Otherwise, the infiltration is clearly faster for the capillaries with longer segments of large width. The shape of the junction has no noticeable effect. The same conclusions can be drawn from the other capillary systems. Comparison with the periodic profiles indicates that the infiltration process is slower (see Figs. 3 and 13), despite the absence of pinning.

Figure 17 shows the results in the presence of misalignment between the upper and lower walls. Misalignment can speed up the infiltration process. As the minimum radius increases, that is, the step ΔH decreases, the effect of misalignment becomes more significant. For smaller segments of the wider part, it is found that misalignment is associated with a weaker resistance to flow (results not shown for brevity). For higher misalignment, when the channels widen, the front remains pinned, creating a plateau. Again, the shape of the junction has no appreciable consequence. We start seeing a clear separation of the curves for smaller minimum radii and higher misalignment: the rectangular shape leads to a slower dynamics. For increasing L_1, it also turns out that the convex shape is associated with a faster infiltration process (not shown for brevity). For periodic profiles, the misalignment of the walls leads to a slightly faster dynamics (see Figs. 5 and 14).

For these capillary systems the reaction has a less marked effect. In Fig. 18 it is instructive to notice that the process of surface growth starts becoming detrimental especially when the front reaches the minimum radius. This observation holds also for the other structures. As a result, the reaction has a higher impact for smaller segments with large radius. The analysis proposed for sinusoidal profiles in order to estimate the effective radius was also performed for the systems of Figs. 17 and 18. It arises that the average radius characterizes the infiltration process better for large minimum radii and high misalignment. Departure from these conditions leads to effective radii closer to the minimum one. For the equivalent sinusoidal profiles the dynamics is faster. Their effective radius is higher. Also the results for the tortuosity indicates that the resistance to flow tends to be stronger for constrictions (results not shown for brevity).

4.2.2 Expansions

Also in this case we restrict ourselves to lengths of 750 lu and widths of $N_y = 125$ lu for the channels. The results for the channels presenting expansions are very interesting for the problem of pinning because it might be presumed that the drag force is weaker while the capillary forces increase because of longer flat walls. From Fig. 19 it can be seen that, for the rectangular shape of the junction, the pinning barrier can not be overcome in any case. For the largest minimum height $H_{\min} = 75$ lu, the front can proceed for the convex geometry. This is easier for the smaller value of L_1. It might appear surprising that the concave geometry can be less favorable. We point out that, for the convex shape, the front has higher momentum when it encounters the sharp corner. For the data of Fig. 19, with $L_1 = 450$ lu, the average over the last three frames before a negative momentum is recorded yields 724 mu·lu/ts for the convex shape and 333 mu·lu/ts for the concave shape. Furthermore, because of the convex geometry, the contact line can slide along the border of the junction and reach again the uniform part of the channel. The penetration for the convex geometry is slightly slower than for constrictions (see Fig. 16). For the sake of completeness, simulations up to $500'000$ ts proves that the pinning barrier is overcome only for the convex geometry with $L_1 = 300,450$ lu and $\Delta H = 25$ lu, corresponding to $H_{\min} = 75$ lu.

Figure 20 shows the results in the presence of misalignment

between the walls. For a rectangular shape of the junction, it is interesting to remark that the misalignment seems to have no effect for $H_{\min} = 50$ lu. The centerline position of the front remains almost unchanged, but the contact line can proceed inside the widening part of the channel. We observe this behavior during a shorter time interval for smaller L_1 (results not shown for brevity). In this case, the capillary forces are expected to be stronger. In the light also of the considerations of the previous paragraph, this configuration can be assumed to be that easing to a larger extent the infiltration. At the beginning, the infiltration process is particularly slow for $H_{\min} = 25$ lu and higher misalignment because the orifice is not behind the contact line. From Fig. 20 we also see that the shape of the junction has no particular influence for $H_{\min} = 75$ lu with misalignment. Also for smaller minimum heights we distinguish no privileged geometry. In general, the effect of misalignment is weaker for longer narrow segments and larger minimum heights. Comparison with constrictions indicates that for wider channels the results are similar (see Fig. 17). Otherwise, constrictions are more interesting for the absence of the phenomenon of pinning. In any case, constrictions can be regarded as expansions for flow in the other sense. So, in a random porous medium, both types of channel are present.

The results with reaction provide a compelling example for the independence of surface growth from the infiltration velocity (see Fig. 21). Comparison with the outcome for constrictions allows to make this statement more precise (see Fig. 18). We see that this is true in particular when the structural features responsible for the retardation of the flow are already behind the contact line. For an extended porous medium, this means that the flow is interrupted because of pore obstruction at the surface of the solid with a relation linear with time. Now, the infiltration velocity is controlled by the pore characteristics. Our finding does not imply that the porous structure is irrelevant. Indeed, a larger porosity should require more time before the flow stops and, on the basis of previous experiments, it might be possible to make predictions. We verified that the curves for z separate more neatly with reactivity for the other values of L_1 and ΔL, since at the beginning both solid steps are behind the contact line for these configurations. Furthermore, the effect of surface growth is more marked for decreasing minimum radii. In general, we recognize no particular influence of the shape of the junction for surface growth.

The infiltration process starts with a strong acceleration near the converging part of the channel, followed by a phase where the front (centerline position) is almost at rest (see Fig. 21). As a consequence, it is more difficult to fit the data to a linear relation. In any case, it follows that the results for expansions are in part comparable with those for constrictions and periodic profiles (sinusoidal and zig-zag) and even slightly faster (see Figs. 9 and 18). The analysis for tortuosity reveals that expansions are less advantageous than constrictions. It also appears that the concave geometry favors infiltration more than the rectangular shape (results not shown for brevity). As an example, for higher misalignment and $H_{\min} = 50$ lu, it is found that the tortuosity is relatively low, around 1.35, with a peak in the range 2-3, when the flow meets the narrowing part of the channel. With reaction, the peaks can reach 5 with stronger reactivity.

5. CONCLUSIONS

Our work deals with LB simulations in 2D for capillary penetration into single channels with walls characterized by different geometric properties. The focus is on the effects for fluid flow of surface growth from a supersaturated solution (Kang et al., 2007, 2002b, 2003, 2004; Lu et al., 2009). The study is motivated by the problem of Si infiltration into C preforms (Bougiouri et al., 2006; Dezellus and Eustathopoulos, 2010; Dezellus et al., 2003; Einset, 1996 and 1998; Eustathopoulos et al., 1999; Hillig et al., 1975; Israel et al., 2010; Liu et al., 2010; Messner and Chiang, 1990; Mortensen et al., 1997; Voytovych et al., 2008). Several inconsistencies exist between the experiments and the models, as well as the simulation conditions. For example, in the LB models the liquid and vapor phases have the same density. But this choice allows to reproduce a linear dynamics for the Washburn infiltration (Chibbaro, 2008; Chibbaro et al., 2009b), as observed in experiments (Israel et al., 2010; Voytovych et al., 2008). However, the accordance with experimental results is poor since in our simulations the Reynolds number is overestimated (Sergi et al., 2014). This shortcoming could be limited by considering longer capillaries with more iterations. This is not necessary for our purposes as the process of surface growth exhibits a relatively weak dependence on the infiltration velocity. This is expected to be the case especially for smaller Reynolds numbers. Furthermore, for interconnected porous systems smaller Reynolds numbers could be attained. Another point is that in our simulations the reaction-rate constant k_r varies, while in real systems this quantity is fixed to a single value. From experimental data the values of the parameter k_r could be chosen more accurately on the basis of the morphology of the growing solid phase at the surface. This kind of analysis is capital because a proper comparison with the experimental results should be based on dimensionless, characteristic numbers involving the time set by the process of pore closure and the corresponding infiltrated distance. Indeed, the flow behavior is expected to depend on the relative effects between the intervening mechanical forces and the speed of reactivity. In this way, it would be possible to have good accordance for the full infiltration dynamics resulting from simulations and experiments. This is easy to understand because otherwise it is imposed only the condition to realize the last stage of the process. Finally, it is worth noticing that other phenomena are even completely disregarded in our description, as thermal effects (Sangsuwan et al., 1999) and the transition to wetting (i.e., the reaction at the contact line). As a consequence, our investigation provides no explanation for the emergence of the linear Washburn behavior (Bougiouri et al., 2006; Israel et al., 2010; Voytovych et al., 2008).

Our modeling approach consists in decomposing intraparticle porosity into basic, simplified structures. Their function for capillary infiltration and surface growth is assessed. Inputs for preform preparation can be singled out. In general,

it is found that the structure of the channels is more important than the minimum radius. More specifically, for periodic profiles, the simulations indicate that the ratio of the amplitude to the channel width, A/N_y, mainly affect the infiltration speed. Smaller ratios are more advantageous. The misalignment between the walls further speeds up the infiltration process. The period does not appear as a prominent parameter. Of course, smaller periods are associated with a higher drag force. For the sinusoidal profiles, the length of the capillaries is not so important, as opposed to uniform channels. Faster infiltration occurs for zig-zag profiles. The results for the sinusoidal profiles are similar. Step-walled capillaries lead to a slower dynamics. In this case, the phenomenon of pinning is more marked.

These considerations have interesting consequences for the selection of ceramic powders and the preform preparation. Small ratios A/N_y can be realized by wide pathways with radius variations weakly pronounced. It follows that powders containing larger particles are good candidates. The results for the misalignment of the walls suggest that an excessive compaction of the grains should be avoided, especially in the direction normal to the infiltration. The use of particles with rounded edges is highly recommended. In particular, the results for step-walled capillaries show that powders with fine grains are detrimental.

Constrictions and expansions can arise by the arrangement of quite coarse particles. By inverting the sense of fluid motion the other configuration is obtained. The danger of pinning associated with expansions should be minor in random porous media given the typical size of the grains. It is interesting to notice that the effect of reaction is weaker for constrictions and expansions. An important consequence is that the flow paths allowing to guide the fluid into the porous structures should be created by means of large aggregates. Small, faceted grains could instead be added in order to enhance the process of surface growth. We recall that in C/SiC composites the SiC formation is desired for the mechanical properties.

To summarize, in order to ensure the impregnation by Si it would thus be advisable to start with preforms presenting pore pathways as wide as possible, straight and with round morphologies. Preferably, this could be achieved by using large ceramic particles. The residual Si in the ceramics could be limited by adding carbon powders containing smaller grains. Particles of small size are likely to slow down the infiltration significantly, in particular if the surface is characterized by corners. Previous investigations have already highlighted the importance of the particle size, the packing properties and the microstructure for the preform to be impregnated (Gadow and Speicher, 2000; Israel et al., 2010; Paik et al., 2002; Salamone et al., 2008). Another finding of relevance is that, especially at the solid surface of the preform, the growth kinetics is expected to depend marginally on the infiltration velocity. As explained, this finding can have practical consequences for the processing conditions (see Sec. 4.2.2). As suggested clearly by the analysis for misalignment, the porosity alone does not characterize exhaustively the whole infiltration process. Our investigation still leaves the open question on the role of the flow pattern inside real porous media for reactive infiltration. Further progress can be made by considering more complex models for the microstructure including interconnected pore channels. Needless to say that this problem is critical for a better determination of the optimal configuration of the porous preform for the manufacturing of ceramic components devised to advanced applications. In that respect, the LB method seems to have an advantage over other numerical schemes for hydrodynamics.

Acknowledgments

The research leading to these results has received funding from the European Union Seventh Framework Programme (FP7/2007-2013) under grant agreement n° 280464, project "High-frequency ELectro-Magnetic technologies for advanced processing of ceramic matrix composites and graphite expansion" (HELM).

[1] Alava M, Dube M, Rost M (2004). Imbibition in disordered media. *Advances in Physics* 53(2):83-175.

[2] Benzi R, Succi S, Vergassola M (1992). The lattice Boltzmann equation: theory and applications. *Physics Reports* 222(3):145-197.

[3] Blow ML, Kusumaatmaja H, Yeomans JM (2009). Imbibition through an array of triangular posts. *Journal of Physics: Condensed Matter* 21(46):464125.

[4] Bougiouri V, Voytovych R, Rojo-Calderon N, Narciso J, Eustathopoulos N (2006). The role of the chemical reaction in the infiltration of porous carbon by NiSi alloys. *Scripta Materialia* 54(11):1875-1878.

[5] Chen S, Doolen GD (1998). Lattice Boltzmann method for fluid flows. *Annual Review of Fluid Mechanics* 30:329-364.

[6] Chibbaro S (2008). Capillary filling with pseudo-potential binary Lattice-Boltzmann model. *The European Physical Journal E* 27(1):99-106.

[7] Chibbaro S, Biferale L, Binder K, Dimitrov D, Diotallevi F, Milchev A, Succi S (2009a). Hydrokinetic simulations of nanoscopic precursor films in rough channels. *Journal of Statistical Mechanics: Theory and Experiments*:6007.

[8] Chibbaro S, Biferale L, Diotallevi F, Succi S (2009b). Capillary filling for multicomponent fluid using the pseudo-potential Lattice Boltzmann method. *The European Physical Journal Special Topics* 171(1):223-228.

[9] Chibbaro S, Costa E, Dimitrov DI, Diotallevi F, Milchev A, Palmieri D, Pontrelli G, Succi S (2009c). Capillary filling in microchannels with wall corrugations: A comparative study of the Concus-Finn criterion by continuum, kinetic, and atomistic approaches. *Langmuir* 25(21):12653-12660.

[10] Clyne TW, Golosnoy IO, Tan JC, Markaki AE (2006). Porous material for thermal management under extreme conditions. *Philosophical Transactions of the Royal Society A* 364(1838):125-146.

[11] Dezellus O, Eustathopoulos N (2010). Fundamental issues of reactive wetting by liquid metals. *Journal of Materials Science* 45(16):4256-4264.

[12] Dezellus O, Hodaj F, Eustathopoulos N (2003). Progress in modelling of chemical-reaction limited wetting. *Journal of the European Ceramic Society* 23(15):2797-2803.

[13] Diotallevi F, Biferale L, Chibbaro S, Lamura A, Pontrelli G, Sbragaglia M, Succi S, Toschi T (2009a). Capillary filling using lattice Boltzmann equations: The case of multi-phase flows. *The European Physical Journal Special Topics* 166(1):111-116.

[14] Diotallevi F, Biferale L, Chibbaro S, Pontrelli G, Toschi F, Succi S (2009b). Lattice Boltzmann simulations of capillary filling: Finite vapour density effects. *The European Physical Journal Special Topics* 171(1):237-243.

[15] Duda A, Koza Z, Matyka M (2011). Hydraulic tortuosity in arbitrary porous media flow. *Physical Review E* 84(3):36319-36326.

[16] Dullien FAL (1992). *Porous Media: Fluid Transport and Pore Structure*, Academic Press.

[17] Einset EO (1996). Capillary infiltration rates into porous media with application to silcomp processing. *Journal of the American Ceramic Society* 79(2):333-338.

[18] Einset EO (1998). Analysis of reactive melt infiltration in the processing of ceramics and ceramic composites. *Chemical Engineering Science* 53(5):1027-1039.

[19] Eustathopoulos N, Nicholas MG, Drevet B (1999). *Wettability at High Temperatures*, Pergamon.

[20] Furler P, Scheffe J, Gorbar M, Moes L, Vogt U, Steinfeld A (2012a). Solar thermochemical CO_2 splitting utilizing a reticulated porous ceria redox system. *Energy and Fuels* 26(11):7051-7059.

[21] Furler P, Scheffe JR, Steinfeld A (2012b). Syngas production by simultaneous splitting of H_2O and CO_2 via ceria redox reactions in a high-temperature solar reactor. *Energy and Environmental Science* 5(3):6098-6103.

[22] Gadow R (2000). Current status and future prospects of CMC brake components and their manufacturing technologies. *24th Annual Conference on Composites, Advanced Ceramics, Materials, and Structures A*, The American Ceramic Society, 15-29.

[23] Gadow R, Speicher M (2000). Optimized morphological design for silicon infiltrated microporous carbon preforms. *24th Annual Conference on Composites, Advanced Ceramics, Materials, and Structures A*, The American Ceramic Society, 485-492.

[24] Gern FH, Kochendörfer R (1997). Liquid silicon infiltration: description of infiltration dynamics and silicon carbide formation. *Composites Part A: Applied Science and Manufacturing* 28(4):355-364.

[25] Ghosh S, Patil P, Mishra SC, Das AK, Das PK (2012). 3-D lattice Boltzmann model for asymmetric Taylor bubble and Taylor drop in inclined channel. *Engineering Applications of Computational Fluid Mechanics* 6(3):383-394.

[26] Goodall R, Mortensen A (2013). Porous metals. *Physical Metallurgy*, Elsevier.

[27] Gross M, Varnik F, Raabe D, Steinbach I (2010). Small droplets on superhydrophobic substrates. *Physical Review E* 81(5):51606-51619.

[28] Grzelakowski C, Jazia DB, Lebeau B, Vonna L, Dupuis D, Haidara H (2009). On the influence of pore structure on the free-imbibition of sessile drops into nanoporous substrates. *Langmuir* 25(10):5855-5860.

[29] Guiet J, Reggio M, Teyssedou A (2011). Implementation and application of the lattice Boltzmann method using MATLAB. *Engineering Applications of Computational Fluid Mechanics* 5(1):117-126.

[30] Haghani R, Rahimian MH, Taghilou M (2013). LBM simulation of a droplet dripping down a hole. *Engineering Applications of Computational Fluid Mechanics* 7(4):461-470.

[31] Hillig WB, Mehan RL, Morelock CR, DeCarlo VJ, Laskow W (1975). Silicon/silicon carbide composites. *American Ceramic Society Bulletin* 54(12):1054-1056.

[32] Israel R, Voytovych R, Protsenko P, Drevet B, Camel D, Eustathopoulos N (2010). Capillary interaction between molten silicon and porous graphite. *Journal of Materials Science* 45(8):2210-2217.

[33] Jeje AA, Zimmermann MH (1979). Resistance to water flow in xylem vessels. *Journal of experimental botany* 30(4):817-827.

[34] Joos P, Van Remoortere P, Bracke M (1990). The kinetics of wetting in a capillary. *Journal of Colloid and Interface Science* 136(1):189-197.

[35] Kang Q, Lichtner PC, Zhang D (2007). An improved lattice Boltzmann model for multicomponent reactive transport in porous media at the pore scale. *Water Resources Research* 43:5551-5562.

[36] Kang Q, Zhang D, Chen S (2002a). Displacement of a two-dimensional immiscible droplet in a channel. *Physics of Fluids* 14(9):3203-3214.

[37] Kang Q, Zhang D, Chen S (2003). Simulation of dissolution and precipitation in porous media. *Journal of Geophysical Research* 108(B10):2504-2513.

[38] Kang Q, Zhang D, Chen S, He X (2002b). Lattice Boltzmann simulation of chemical dissolution in porous media. *Physical Review E* 65(3):36318-36325.

[39] Kang Q, Zhang D, Lichtner PC, Tsimpanogiannis IN (2004). Lattice Boltzmann model for crystal growth from supersaturated solution. *Geophysical Research Letters* 31:21107-21111.

[40] Krenkel W (2005). Carbon fibre reinforced silicon carbide composites (C/SiC, C/C-SiC). *Handbook of Ceramic Composites*, Kluwer Academic Publisher, 117-48.

[41] Kusumaatmaja H, Pooley CM, Girardo S, Pisignano D, Yeomans JM (2008). Capillary filling in pattern channels. *Physical Review E* 77(6):67301-67304.

[42] Landau LD, Lifshitz EM (2008). *Fluid Mechanics*, Elsevier.

[43] Liu GW, Muolo ML, Valenza F, Passerone A (2010). Survey on wetting of SiC by molten metals. *Ceramics International* 36(4):1177-1188.

[44] Lu G, DePaolo DJ, Kang Q, Zhang D (2009). Lattice Boltzmann simulation of snow crystal growth in clouds. *Journal of Geophysical Research* 114:11087-11100.

[45] Martys NS, Hagedorn JG (2002). Multiscale modeling of fluid transport in heterogeneous materials using discrete Boltzmann methods. *Materials and Structures* 35(10):650-659.

[46] Matyka M, Koza Z (2012). How to calculate tortuosity easily? *American Institute of Physics Conference Proceedings* 1453, 17-22.

[47] Messner RP, Chiang YM (1990). Liquid-phase reaction-bonding of silicon carbide using alloyed silicon-molybdenum melts. *Journal of the American Ceramic Society* 73(5):1193-1200.

[48] Miller W, Succi S (2002). A lattice Boltzmann model for anisotropic crystal growth from melt. *Journal of Statistical Physics* 107(1-2):173-186.

[49] Mognetti BM, Yeomans JM (2009). Capillary filling in microchannels patterned by posts. *Physical Review E* 80(5):56309-56316.

[50] Mortensen A, Drevet B, Eustathopoulos N (1997). Kinetics of diffusion-limited spreading of sessile drops in reactive wetting. *Scripta Materialia* 36(6):645-651.

[51] Ota T, Takahashi M, Hibi T, Ozawa M, Suzuki S, Hi-

kichi Y, Suzuki H (1995). Biomimetic process for producing SiC "Wood". *Journal of the American Ceramic Society* 78(12):3409-3411.

[52] Paik U, Park HC, Choi SC, Ha CG, Kim JW, Jung YG (2002). Effect of particle dispersion on microstructure and strength of reaction-bonded silicon carbide. *Materials Science and Engineering: A* 334(1-2):267-274.

[53] Pan C, Hilpert M, Miller CT (2004). Lattice-Boltzmann simulation of two-phase flow in porous media. *Water Resources Research* 40(1):1501-1514.

[54] Patro D, Bhattacharyya S, Jayram V (2007). Flow kinetics in porous ceramics: understanding with non-uniform capillary models. *Journal of the American Ceramic Society* 90(10):3040-3046.

[55] Quéré D (2008). Wetting and roughness. *Annual Review of Materials Research* 38:71-99.

[56] Roberts AP, Garboczi EJ (2000). Elastic properties of model porous ceramics. *Journal of the American Ceramic Society* 83(12):3041-3048.

[57] Salamone S, Karandikar P, Marshall A, Marchant DD, Sennett M (2008). Effects of SI:SiC ratio and SiC grain size on properties for RBSC. *Mechanical Properties and Performance of Engineering Ceramics and Composites III*, Wiley, 101-109.

[58] Sangsuwan P, Tewari SN, Gatica JE, Singh M, Dickerson R (1999). Reactive infiltration of silicon melt through microporous amorphous carbon preforms. *Metallurgical and Materials Transaction B* 30B(5):933-944.

[59] Schaap MG, Porter ML, Christensen BSB, Wildenschild D (2007). Comparison of pressure-saturation characteristics derived from computed tomography and lattice Boltzmann simulations. *Water Resources Research* 43(12):6-20.

[60] Sergi D, Grossi L, Leidi T, Ortona A (2014). Surface growth effects on reactive capillary-driven flow: lattice Boltzmann investigation. *Engineering Applications of Computational Fluid Mechanics*, to be published.

[61] Shan X, Chen H (1993). Lattice Boltzmann model for simulating flows with multiple phases and components. *Physical Review E* 47(3):1815-1819.

[62] Shan X, Doolen GD (1995). Multicomponent lattice-Boltzmann model with interparticle interaction. *Journal of Statistical Physics* 81(1-2):379-393.

[63] Studart AR, Gonzenbach UT, Tervoort E, Gauckler LJ (2006). Processing routes to macroporous ceramics: a review. *Journal of the American Ceramic Society* 89(6):1771-1789.

[64] Succi S (2009). *The Lattice Boltzmann Equation for Fluid Dynamics and Beyond*, Oxford University Press.

[65] Sukop MC, Or D (2004). Lattice Boltzmann method for modeling liquid-vapor interface configurations in porous media. *Water Resources Research* 40(1):1509-1519.

[66] Sukop MC, Thorne Jr DT (2010). *Lattice Boltzmann Modeling: An Introduction for Geoscientists and Engineers*, Springer.

[67] Svihla CK, Hong X (2006). Simulation of free surface flows with surface tension with ANSYS CFX. *2006 International ANSYS Conference*. Pittsburgh, USA.

[68] Trimis D, Pickenäcker O, Wawrzinek K (2006). Porous burners. *Cellular Ceramics: Structure, Manufacturing, Properties and Applications*, Wiley-VCH, 484-508.

[69] Van Remoortere P, Joos P (1993). About the kinetics of partial wetting. *Journal of Colloid and Interface Science* 160(2):387-396.

[70] Voytovych R, Bougiouri V, Calderon NR, Narciso J, Eustathopoulos N (2008). Reactive infiltration of porous graphite by NiSi alloys. *Acta Materialia* 56(10):2237-2246.

[71] Wagner AJ (2003). The origin of spurious velocities in lattice Boltzmann. *International Journal of Modern Physics B* 17(1-2):193-196.

[72] Wiklund H, Uesaka T (2012). Edge-wicking: micro-fluidics of two-dimensional liquid penetration into porous structures. *Nordic Pulp and Paper Research Journal* 27(2):403-408.

[73] Wiklund HS, Uesaka T (2013). Microfluidics of imbibition in random porous media. *Physical Review E* 87(2):23006-23014.

[74] Wolf-Gladrow DA (2005). *Lattice-Gas Cellular Automata and Lattice Boltzmann Models - An Introduction*, Springer.

[75] Xu H, Guetary C (2004). The use of CFD to simulate capillary rise and comparison to experimental data. *2004 International ANSYS Conference*. Pittsburgh, USA.

[76] Zeschky J, Höfner T, Arnold C, Weissmann R, Bahloul-Hourlier D, Scheffler M, Greil P (2005). Polysilsesquioxane derived ceramic foams with gradient porosity. *Acta Materialia* 53(4):927-937.